# Mitofusin 2 regulates neutrophil adhesive migration via suppressing Rac activation

Wenqing Zhou[1], Alan Hsu[1], Tianqi Wang[1], Jacob Jeffries[1], Haroon Mohammad[2], Xu Wang[3,4], David Umulis[3,4], Mohamed N. Seleem[2], Qing Deng[1,5,6*]

1. Department of Biological Sciences, Purdue University, West Lafayette, IN 47907 USA
2. Department of Comparative Pathobiology, Purdue University, West Lafayette, IN 47907 USA
3. Department of Agricultural & Biological Engineering, Purdue University, West Lafayette, IN 47907 USA
4. Weldon School of Biomedical Engineering, Purdue University, West Lafayette, IN 47907 USA
5. Purdue Institute for Inflammation, Immunology, & Infectious Disease, Purdue University, West Lafayette, IN 47907 USA
6. Purdue University Center for Cancer Research, Purdue University, West Lafayette, IN 47907 USA

*Corresponding author:
G231 Biological Sciences
Purdue University
915 W. State Street
West Lafayette, IN 47907
Tel: 765-494-0423
Fax: 765-494-0876
deng67@purdue.edu

## Abstract

Mitochondrial membrane potential is required for neutrophil migration, although the mechanism remains unclear. Here, we report that mitochondrial outer membrane protein Mitofusin 2 (Mfn2) regulates neutrophil homeostasis in vivo. *Mfn2*-deficient neutrophils are released from the hematopoietic tissue and trapped in the vasculature in zebrafish embryos. Human neutrophil-like cells deficient with MFN2 fail to be arrested by activated endothelium under sheer stress or perform chemotaxis on substrates. Deletion of Mfn2 results in a significant reduction of neutrophil infiltration to the inflamed peritoneal cavity in mice. *Mfn2*-deficient neutrophil-like cells and mouse embryonic fibroblasts display heightened Rac activation. Mechanistically, MFN2 maintains mitochondria-ER interaction and prevents excessive elevation of cytosolic calcium and subsequent phosphorylation of CaMKII upon stimulation. Inhibiting CaMKII or the Rac GEF Tiam rescues the chemotaxis defect that results from Mfn2 depletion. Altogether, we identified an Mfn2-CaMKII-Tiam-Rac axis in regulating neutrophil migration and discovered a role of *MFN2* in regulating the actin cytoskeleton.

## Introduction

Neutrophils, the most abundant circulating leukocytes in humans, constitute the first line of host defense. Upon stimulation by either pathogen or host-derived proinflammatory mediators, neutrophils are recruited to inflamed tissue using spatially and temporally dynamic intracellular signaling pathways. Activation of the surface receptors, primarily the G-protein-coupled receptors[1-4], leads to the activation of phosphatidylinositol 3-kinases (PI3K) that produces

phosphatidylinositol (3,4,5)P3 and activates small GTPases such as Rac. Rac promotes actin polymerization at the leading edge and drives cell migration[5]. In parallel, G-protein-coupled receptors activate phospholipase C, which generates IP3 and activates the $Ca^{2+}$ release from intracellular stores[6]. Although intracellular $Ca^{2+}$ is a well characterized second messenger that activates Rac and regulates cell migration in slowly migrating cells[6, 7], its role in neutrophil migration is less clear.

Cell migration requires the coordination of multiple cellular organelles, including mitochondria. Mitochondria carry out oxidative phosphorylation to produce ATP and regulate the intracellular redox status and intracellular distribution of $Ca^{2+}$ that are both involved in cell migration. In addition, mitochondria morphology changes via fusion and fission[8] to adapt to variable metabolic needs under different conditions. Mitochondria fission is believed to promote cell migration by providing localized mitochondria and ATP production[9, 10].

In neutrophils, mitochondrial biology is distinct and contradictory. The Warburg effect is well-documented in neutrophils that they primarily use glycolysis for ATP generation[11]. Neutrophils have a relative low number of mitochondria, low respiration rates and low enzymatic activity of the electron transport chain[12]. However, maintaining mitochondria membrane potential is still required for chemotaxis. Disrupting mitochondria membrane potential by pharmacological inhibitors abolished chemotaxis of isolated primary neutrophils[13-15]. Although mitochondria-derived ATP possibly regulates neutrophil chemotaxis in vitro[15], removal of extracellular ATP actually improves neutrophil chemotaxis in vivo[16]. These conflicting reports prompted us to

search for mechanisms delineating the role of mitochondria in neutrophil migration outside the realm of ATP or cellular energy[17-19].

Neutrophils are terminally differentiated and undergo apoptosis within 24 hours in culture and thus are not genetically tractable. We have overcome this hurdle by developing a neutrophil-specific knockout platform in zebrafish[20]. The zebrafish is a suitable model for neutrophil research because of its highly conserved innate immune system. In our previous work, we have confirmed the requirement of mitochondrial membrane potential, biosynthesis and electron transport chain in the migration of zebrafish neutrophils[20]. In addition, we have visualized a highly fused tubular network of mitochondria in zebrafish neutrophils, which is consistent with a previous report investigating primary human neutrophils[21]. Here we present evidence that Mitofusin 2 (Mfn2) regulates Rac activation to coordinate neutrophil adhesive migration. In addition, we reveal a previously unknown function of Mfn2 in regulating the actin cytoskeleton, contributing to the understanding and management of patients with mitochondrial diseases.

## Results

### Neutrophils depleted with *mfn2* accumulate in zebrafish vasculature

Here, we address whether a highly fused mitochondrial network benefits neutrophil migration by targeting and disrupting proteins that regulate mitochondrial shape in zebrafish neutrophils. Mitofusins Mfn1 and Mfn2 are required for mitochondrial outer membrane fusion[22] and Opa1

regulates inner membrane fusion[23]. In embryos produced from the transgenic line we generated, *Tg(lyzC:Cas9-mfn2 sgRNAs)*$^{pu23}$, that expresses two independent sgRNAs targeting *mfn2*, the majority of neutrophils circulate in the bloodstream (Fig. 1a, b and Supplementary Movie 1). This is in sharp contrast to the control or the wild-type embryos where over 99% of neutrophils are retained in the caudal hematopoietic tissue or in the head mesenchyme[24]. This abnormal distribution of neutrophils was further confirmed in a second transgenic line expressing a different set of sgRNAs targeting *mfn2*, *Tg(lyzC:Cas9-mfn2 sgRNAs#2)*$^{pu24}$ (Fig. 1a, b and Supplementary Movie 2). Neutrophils were sorted from both lines and their respective loci targeted by the 4 sgRNAs were deep sequenced. The overall mutation frequency ranged from 24% to 60%. In contrast, circulating neutrophils were not observed in embryos expressing sgRNAs targeting *opa1*, although the velocity of neutrophil migration in the head mesenchyme was significantly reduced (Supplementary Fig. 1 and Supplementary Movie 3), indicating that decreased neutrophil retention in tissue is not simply due to defects in mitochondrial fusion.

Next, we determined whether neutrophils in the vasculature were able to respond to acute inflammation induced by a tail transection or performing chemotaxis to $LTB_4$. Significant defects in both assays were observed in the line with neutrophil specific *mfn2* deletion (Fig. 1c-f, d and Supplementary Movie 4). Taken together, *mfn2* regulates neutrophil tissue retention and extravasation in zebrafish.

**MFN2 regulates adhesion and adhesive migration in human neutrophil-like cells**

To get to the mechanism how Mfn2 regulates neutrophil migration, we knocked down MFN2 in human neutrophil-like cells, HL-60, using shRNAs and obtained two individual lines with 80% and 50% reduction of MFN2(Fig. 2a). No difference in apoptosis or cell maturation was noticed in the cell lines (Supplementary Fig. 2). First, we measured neutrophil static adhesion to fibrinogen-coated substrates. Differentiated HL-60 cells (dHL-60) expressing one shRNA targeting *MFN2* (*MFN2-sh1)* displayed significantly decreased adhesion in the absence or presence of N-Formylmethionyl-leucyl-phenylalanine (fMLP) (Fig. 2b). The second shRNA *MFN2-sh2* also caused a slight reduction in neutrophil adhesion. To recapitulate the phenotype in zebrafish where neutrophils depleted with *mfn2* failed to adhere to the vasculature, we measured cell adhesion to activated endothelial cells under shear stress. A majority of *MFN2*-deficient cells failed to adhere to endothelial cells. A small fraction of cells rolled on top of endothelial cell but failed to arrest, suggesting a defect in forming tight adhesions (Fig. 2c, d and Supplementary Movie 5). We then used IBIDI chemotaxis slides to determine whether *MFN2* is required for neutrophil chemotaxis on collagen coated 2-dimensional surfaces that require cell adhesion for taxis. As expected, both shRNAs interfered with neutrophil chemotaxis towards fMLP (Fig. 3a, b). To further validate the specificity of the shRNA, a sh1 resistant *MFN2* was introduced to the knock down cells and indeed the defect in chemotaxis was rescued (Fig. 3c-e and Supplementary Movie 6). Intriguingly, when we knocked down MFN1 that shares a similar structure and function with MFN2 in dHL-60 cells, we found no defects in chemotaxis (Supplementary Fig. 3 and Supplementary Movie 7). To investigate whether Mfn2 is required for neutrophil infiltration in mice, we bred *Mfn2* flox/flox mice[25] with the *S100A8-Cre* strain[26] for neutrophil specific depletion. With 50% of Mfn2 protein reduction in neutrophils obtained in this strain, significant reduction of neutrophil infiltration into the inflamed peritoneal cavity was observed (Fig. 3f, g).

Blood cell composition was not altered by Mfn2 depletion (28% and 32% granulocytes in the *Cre*$^{+}$ and *Cre*$^{-}$ lines, respectively), consistent with a previous report that *Mfn2* does not regulate blood cell development under hemostatic conditions[27]. Therefore, MFN2 is required for neutrophil chemotaxis and infiltration in mammals.

**Mfn2 regulates the actin cytoskeleton and migration of mouse embryonic fibroblasts**

In addition to neutrophils, we investigated the function of Mfn2 in mouse embryonic fibroblasts (MEF). *Mfn2-null* MEFs are round with enriched actin filaments and Paxillin in the cell cortex, whereas *wt* MEFs are elongated with stress fibers when plated on both ligand-coated and uncoated substrates (Fig. 4a and Supplementary Fig. 4a, b). *Mfn1*-deficient MEFs were round but retained stress fibers (Supplementary Fig. 4c, d). The significant changes in actin organization suggest that *Mfn2-null* MEFs may migrate differently. Indeed, MEFs deficient with Mfn2 migrated slower when compared to *wt* cells during wound closure (Fig. 4c, d and Supplementary Movie 8). In addition, right after plating, *wt* MEFs extended transient filopodia and lamellipodia and eventually elongated, whereas *Mfn2-null* MEFs generated extensive membrane ruffles and retained the circular shape (Fig. 4d and Supplementary Movie 9). *Mfn1-null* cells spread similarly to the *wt* cells (Supplementary Fig. 4e). In summary, Mfn2 modulates the actin cytoskeleton and cell migration in MEFs.

**MFN2 suppresses RAC activation**

The predominant cortical actin, nascent focal contacts and extensive membrane ruffles in *Mfn2-null* MEF cells (Fig. 4) resembled the classic phenotype of fibroblasts expressing the constitutively active Rac[28], indicating that Mfn2 may negatively regulate Rac activation. We therefore performed a RAC-GTP pull-down to measure RAC activation in *MFN2*-deficient dHL-60 cells. Significantly increased amount of active RAC were detected in *MFN2-sh1* cells 5 min after fMLP stimulation (Fig. 5a, b). RAC-GTP colocalized with F-actins at cell protrusions as well as the retracting rear of the cells (Fig. 5c) and the lamellipodia in the *MFN2-sh1* cells accumulated more active RAC than that in the control cells. To determine whether RAC over activation contributes to the chemotaxis defect in *MFN2*-deficient dHL-60 cells, a RAC inhibitor NSC23766 was utilized. NSC23766 restored neutrophil adhesive migration in *MFN2-sh1* cells, at least partially, at a concentration that did not affect chemotaxis of control cells (Fig. 5d, e, and Supplementary Movie 10), suggesting that MFN2 regulates neutrophil migration through suppressing RAC activation.

**Mfn2 regulates mitochondria-ER tethering and calcium signaling in dHL-60 cells**

We next investigated how MFN2 regulates RAC activation in neutrophils. Mfn2 localizes to both mitochondria and the ER membrane and regulates the tethering between the two organelles in MEF[29]. To determine whether MFN2 mediates mitochondria-ER tethering in neutrophils, we determined the distribution of MFN2 in dHL-60 cells. MFN2 colocalized with both the mitochondria (stained with a TOMM20 antibody) and the ER (stained with a CALNEXIN antibody), and the Manders' colocalization coefficiency was 0.60±0.085 and 0.69±0.13, respectively (Fig. 6a, b). Mitochondria colocalized with the ER (Manders' colocalization

coefficiency 0.52±0.097) and distributed throughout the cell body (Fig. 6a, b). The morphology of the mitochondria and the ER was also visualized using electron microscopy in dHL-60 cells (Supplementary Fig. 5). When MFN2 was inhibited, mitochondria lost their structure and accumulated in the middle of the cell body and formed a clumpy structure similar to that in Mfn2 KO MEFs[22]. Together, these results suggest that MFN2 mediates mitochondria-ER tethering in neutrophils.

The close proximity of the ER and the mitochondria regulates multiple cellular signaling pathways including calcium homeostasis[30]. Indeed, *MFN2*-deficient dHL-60 cells exhibited higher levels of cytosolic $Ca^{2+}$ and reduced mitochondrial $Ca^{2+}$ levels after fMLP stimulation (Fig. 6c, d). Furthermore, mitochondrial membrane potential and the ROS level in mitochondria were also reduced when MFN2 was depleted, especially post fMLP stimulation (Supplementary Fig. 6a-d). This is consistent with the notion that mitochondrial $Ca^{2+}$ activates the electron transportation chain[31]. On the contrary, the ATP levels were not affected in the MFN2 knock down dHL-60 cells (Supplementary Fig. 6e), in line with the observation that mitochondria are not a major source of ATP in neutrophils[11, 32]. We attempted to buffer cytosolic $Ca^{2+}$ using BAPTA to determine whether elevated cytosolic $Ca^{2+}$ is responsible for the chemotaxis defects in MFN2 knock down cells. However, a global cytosolic $Ca^{2+}$ inhibition abrogated the ability of dHL-60 to migrate (Supplementary Fig. 7), consistent with the previous observation that cytosolic $Ca^{2+}$ possibly is tightly regulated spatially and/or temporally for neutrophil migration[33, 34]. In summary, depletion of *MFN2* alters cellular $Ca^{2+}$ homeostasis but not ATP levels in neutrophils.

**MFN2 orchestrates the activation of CaMKII and TIAM2 to control neutrophil migration**

Our data so far suggested that MFN2 regulates neutrophil adhesion to endothelium and adhesive migration, via suppressing Rac over-activation and possibly excessive levels of cytosolic $Ca^{2+}$. In the literature, several pathways have been identified to link cytosolic $Ca^{2+}$ to focal adhesion dynamics and Rho GTPases. In fibroblasts, elevated $Ca^{2+}$ facilitates focal adhesion disassembly by triggering the activation of $Ca^{2+}$/calmodulin-dependent protein kinase, CaMKII[35]. CaMKIIγ is the predominant form of CaMKII in HL-60 cells which regulates differentiation of myeloid leukemia cells[36]. However CaMKII's role in neutrophil adhesion or migration is not characterized. We first visualized the active, phosphorylated CaMKII and focal complexes in polarized control and *MFN2* knock down dHL-60 cells. The number of PAXILLIN positive adhesion complexes was reduced in *MFN2*-depleted cells, especially at the cell front (Fig. 7a, b). Furthermore, the activated phosphorylated CaMKII colocalized with PAXILLIN and was significantly increased in *MFN2*-depleted cells (Fig. 7a, c). In addition, AIP, an inhibitor targeting the catalytic activity of CaMKII, was able to restore cell adhesive migration in *MFN2*-deficient cells, at least partially (Fig. 7e, f and Supplementary Movie 11), indicating that MFN2 regulates the activation of CaMKII in neutrophils.

CaMKII phosphorylates Tiam1, a guanine nucleotide exchange factor of Rac, and enhances its nucleotide exchange activity, although the phosphorylation sites are unknown[37]. Tiam1 promotes focal adhesion disassembly in fibroblasts[38]. In primary murine neutrophils, Tiam2 regulates cell

motility also by triggering focal adhesion disassembly[39]. We next assessed the function of TIAM2 in our system. TIAM2 formed puncta that colocalized with PAXILLIN which is distributed throughout the cell body including the leading edge of dHL-60 cells (Fig. 7d). The TIAM inhibitor CAS1090893 restored adhesive migration in *MFN2* depleted cells (Fig. 7e, f and Supplementary Movie 11). Altogether, our data support a model that MFN2 suppresses the level of elevated cytosolic $Ca^{2+}$ upon chemokine stimulation. Excessive $Ca^{2+}$ in turn triggers over activation of CaMKII and its downstream target TIAM2, leading to RAC-mediated focal adhesion disassembly and impaired neutrophil adhesion (Fig. 7g).

## Discussion

Here we report that Mfn2 is crucial for neutrophil adhesion and adhesive migration, providing evidence that Mfn2 regulates the actin cytoskeleton and cell migration. By maintaining the tether between the mitochondria and ER, Mfn2 orchestrates intracellular $Ca^{2+}$ signaling and regulates Rac activation. We also provide evidence that the $Ca^{2+}$-dependent kinase CaMKII and its substrate Tiam2 are downstream effectors of Mfn2, regulating the activation of Rac in neutrophils to modulate the stability of focal adhesion and cell migration. Therefore, we have identified the mechanism for how Mfn2 regulates neutrophil adhesive migration, and highlighted the importance of mitochondria and their contact with the ER in neutrophils.

Studies using knockout mice and cell culture have concluded that Mfn1 and Mfn2 possess unique functions, although both mediate mitochondrial outer membrane fusion[22]. Our data that only MFN2, but not MFN1, is required for neutrophil adhesive migration supports that

mitochondrial fusion is not likely important for neutrophil migration. Our observation goes against a body of literature that mitochondrial fission promotes cell migration in other cell types[9, 10]. Alternatively, we propose a model that, in neutrophils, the interaction of mitochondria with the ER is more critical than a fused network. Although MFN2 is not the only protein that can mediate the mitochondria-ER tether[40], mitochondria and ER interaction was significantly reduced upon MFN2 deletion in dHL-60, suggesting that MFN2 is at least one of the critical tether proteins in neutrophils. The fused network of mitochondrial network in neutrophils is possibly a result of the abundant expression of the mitofusins. Mutations in human MFN2 cause Charcot-Marie-Tooth disease type 2A (CMT2A), a classical axonal peripheral sensorimotor neuropathy[41]. MFN2 is also implicated in many other diseases such as cancer, cardiomyopathies, diabetes and Alzheimer's disease[42]. Currently, over 100 dominant mutations in the *MFN2* gene have been reported in CMT2A patients though how these mutations lead to disease is still largely unknown. The challenges in MFN2 research are that MFN2 regulates mitochondrial fusion and a plethora of cellular functions such as mitochondrial dynamics, transport, mtDNA stability, lipid metabolism and survival[43]. In addition, gain-of-function and loss-of-function mutations are reported that affect different aspects of cellular functions[43]. Our findings provide a new direction to understand the consequences of MFN2 deficiency in disease pathology, namely the actin cytoskeleton and Rac. Our findings also imply a possibility that the defect in immune cell migration in humans may affect immunity or chronic inflammation and regulate the progression of the aforementioned diseases. Future work will be required to carefully evaluate the individual mutations of MFN2 identified in human diseases in immune cell migration. It is possible that mutations disrupting mitochondria-ER tethering, but not membrane fusion, result in defects in regulating cell adhesion and the cytoskeleton.

Our conclusions present a significant departure from the prevailing focus of bioenergy, in other word ATP, in cell migration. In many cell types, including neutrophils, the relevance of mitochondria-derived ATP in cell migration is emphasized[14, 15]. A recent report has confirmed the established literature that mitochondria do not provide ATP in neutrophils[32]. Intriguingly, OPA1 deletion suppresses the production of neutrophil extracellular traps and alters the cellular ATP levels by indirectly suppressing glycolysis. In contrast, MFN2 deletion does not affect ATP levels (Supplementary Fig. 6) or affect neutrophil extracellular trap formation[32], suggesting again distinct biological functions of OPA1 and MFN2, although both proteins regulate mitochondrial shapes. In vascular endothelial cells, mitochondria also serve as signaling rather than energy-producing moieties[44]. In our study, in addition to the altered $Ca^{2+}$ level, mitochondrial membrane potential and ROS, both critical for neutrophil chemotaxis and migration[13, 20], were reduced in stimulated *MFN2*-deficient dHL-60 cells. It remains to be determined whether the modest decreases in mitochondria membrane potential or ROS contribute to the defect of neutrophil migration upon MFN2 deletion.

Cell migration requires temporally and spatially regulated distribution of cytoskeleton networks, adhesion structures[45] and Rho family GTPases. During neutrophil migration, Rac is well appreciated to localize to the front of cells[46] where it nucleates branched actin to generate lamellipodia and membrane protrusion[47]. Recently, Fayngerts *et al* have developed a method to stain Rac-GTP and concluded that Rac-GTP enriches at the leading edge in both murine neutrophils and dHL-60 cells[48], without F-actin or other leading edge marker co-stained. In our current study, we observed a similar pattern of Rac-GTP staining, but noticed that active Rac

does not necessarily localize to cell protrusions labeled with F-actin. This observation is also in line with live neutrophil imaging using Rac FRET reporter mice where Rac activation oscillates between cell front and rear[49]. The function of Rac in the cells is possibly related to its ability to trigger focal adhesion disassembly[50, 51]. Nascent adhesions and focal complexes, prominent in highly motile cells like leukocytes (reviewed in[52]), may be required to generate an anchor for the polymerizing actin to overcome the membrane tension which allows cells to move forward. Integrin-mediated adhesions also dissemble at the rear to allow tail detachment. Conceptually, it makes sense that Rac is activated at both the front and rear to dissemble adhesion structures to regulate cell migration.

In neutrophils, there are four families of Rac-GEFs, including the Dbl-type P-Rex, Vav, Tiam and a structurally-unrelated DOCK family, with the Tiam2 least characterized[4]. Tiam1 localizes to focal adhesions via direct binding to Talin where it mediates Rac activation and promotes cell spreading and adhesion turnover[53]. In our study, we observed fewer focal adhesions in *MFN2*-deficient neutrophils. The pharmacological inhibitor CAS1090893, which disrupts the interaction between Tiam and Rac, reversed the migration defect of *MFN2*-deficient neutrophils, indicating that Tiam is regulated by MFN2 in neutrophils. Indeed, blocking Tiam2 stimulated focal complex formation in murine neutrophils[39] and skin papilloma cells[38]. In addition, constitutively-active Tiam2 led to accumulation of adhesion structures around the cell periphery[38], a phenotype also observed in *Mfn2-null* MEFs, further supporting that Tiam is over activated in cells lacking Mfn2.

Our result in leukocyte is consistent with previous work in murine fibroblasts[30] that knocking out Mfn2 results in excessive cytosolic $Ca^{2+}$ and defective mitochondrial calcium uptake. Intriguingly, blocking mitochondrial calcium import by inhibiting the mitochondria uniporter resulted in the reduction of the ER and cytosolic $Ca^{2+}$ pools and a migration defect[54], albeit with different mechanisms. It has been well-established that elevation of $Ca^{2+}$ induces focal adhesion disassembly in multiple cell types[55, 56], although the mechanism is less clear. In neutrophils, it was noted that cytosolic $Ca^{2+}$ is required for neutrophils to detach from the substrates[34]. Our results suggest that the CaMKII-Tiam2-Rac axis is a major pathway regulated by Mfn2 and cytosolic $Ca^{2+}$ to regulate focal adhesion disassembly and neutrophil migration. Although cytosolic $Ca^{2+}$ triggers the activation of Rac[57], previous work in neutrophils suggests that Rac activation was independent of cytosolic $Ca^{2+}$[57, 58]. This discrepancy could be explained with the differences in assay conditions (suspension vs. adhesion) or $Ca^{2+}$ levels (elevation vs. reduction). It remains to be determined which residues on Tiam2 are phosphorylated by CaMKII that lead to a conformational change and activation of Tiam family GEFs[59]. Additional characterizations are also needed to determine whether other calcium sensitive molecules, such as Calcineurin, myosin light chain kinase, PKC/RhoGAP and Calpain[57, 60-62], are regulated by Mfn2 to regulate focal adhesion dynamics in neutrophils.

In summary, by suppression of Mfn2 in different models, we have discovered an essential role Mfn2 plays in neutrophil adhesion and migration, and determined the downstream mechanism, which may provide insights and potential therapeutic strategies for the treatment of inflammatory diseases and mitochondrial diseases.

## Online Methods

### Animals

The zebrafish and mice experiments were conducted in accordance to the internationally accepted standards. The Animal Care and Use Protocols were approved by The Purdue Animal Care and Use Committee (PACUC), adhering to the Guidelines for Use of Zebrafish and Mice in the NIH Intramural Research Program (Protocol number: 1401001018 and 1803001702, respectively).

To generate transgenic zebrafish lines, plasmids with the tol2 backbone were coinjected with Tol2 transposase mRNA into embryos of the AB strain at one-cell stage as described[63].

Constructs for neutrophil-specific knock out in zebrafish were generated as described[63] using the following primers (guide RNA sequences were indicated with underscores):

mfn2 guide1-F1:

GTGGATGAGCTGCGGGTGGGTTTAAGAGCTATGCTGGAAACAGCATAGC mfn2 guide1-R1: CGCACCTCCGCCACCTGCCCGAACTAGGAGCCTGGAGAACTGC

mfn2 guide1-F2: GGTGGCGGAGGTGCGGTTTAAGAGCTATGCTGGAAACAGCATAGC

mfn2 guide1-R2: CCGCAGCTCATCCACCGAACCAAGAGCTGGAGGGAGA

mfn2 guide2-F1:

GGGGGATACCTGTCCAAAGGTTTAAGAGCTATGCTGGAAACAGCATAGCAAG

mfn2 guide2-R1:

AGACCTTCCTCTATGTGCCCGAACTAGGAGCCTGGAGAACTGCTATATAAAC

mfn2 guide2-F2:

CATAGAGGAAGGTCTGTTTAAGAGCTATGCTGGAAACAGCATAGCAAGTTTAAATA

AG

mfn2 guide2-R2:

GGACAGGTATCCCCCCGAACCAAGAGCTGGAGGGAGAGCTATATATAC opa1 guide-

F1: GTAGTTGGGGACCAGAGTGGTTTAAGAGCTATGCTGGAAACAGCATAGC opa1

guide-R1: CCTCACTGCTCAGCTGCCCGAACTAGGAGCCTGGAGAACTGC

opa1 guide-F2: AGCTGAGCAGTGAGGGTTTAAGAGCTATGCTGGAAACAGCATAGC

opa1 guide-R2: CTGGTCCCCAACTACCGAACCAAGAGCTGGAGGGAGA

All mice used in this study were purchased from Jackson Laboratories. Conditional *Mfn2* knockout mice (B6.129(Cg)-*Mfn2*$^{tm3Dcc}$/J) were crossed to S100A8-Cre (B6.Cg-Tg(S100A8-cre, -EGFP)1Ilw/J) transgenic mice to obtain a homozygous floxed *Mfn2* alleles with or without the Cre. All mice were used at age 6-12 weeks, and both male and female were used for experiments.

**Cell Culture**

A clonal HL-60 line was a generous gift from Dr. Orion D. Weiner (UCSF). HEK293T, *wild-type*, *Mfn2-null* and *Mfn1-null* MEFs were purchased from American Type Culture Collection (ATCC). HUVEC was from Sigma-Aldrich (200P-05N). All cells were maintained in their specific media at 37°C with 5% $CO_2$. HL-60 cells were cultured in RPMI-1640 (Corning) with 10% FBS (Minipore), 25 mM HEPES, 1% sodium bicarbonate, and 1% sodium pyruvate. HEK293T and MEF cells were cultured in 10%FBS, 4.5g/glucose DMEM (Corning) with sodium bicarbonate. HUVEC was cultured in Endothelial cell Growth Media (R&D SYSTEMS,

CCM027). HL-60 cells were differentiated with 1.5% DMSO for 5-6 days. Cells were checked monthly for mycoplasma using the e-Myco plus Mycoplasma PCR Detection Kit (Bulldog Bio 25234).

To generate knocking down lines in HL-60 cells, pLKO.1 lentiviral constructs with shRNA was obtained from Sigma-Aldrich (*MFN2-sh1*:TRCN0000082684, *MFN2-sh2*: TRCN0000082687, *MFN1-sh*: TRCN0000051837), and SHC 003 was used as a non-targeting control. MFN2 rescue construct was generated by replacing GFP with *sh1*-resistant *MFN2*. Primers MFN2r-F: CAAGTGTATTGTGAAGAGATGCGTGAAGAGCGGCAAG and MFN2r-R: TTCACAATACACTTGTTGCTCCCGAGCCGCCATG was used to make *sh1*-resistant *MFN2* with Mfn2-YFP (addgene #28010) as the template. Primers pLKO-F: AATTCTCGACCTCGAGACAAATGGC and pLKO-R: GGTGGCGACCGGGAGCGC were used to linearize the backbone of pLKO, and p-MFN2r-F: CTCCCGGTCGCCACCATGTCCCTGCTCTTCTCTCG and p-MFN2r-R: TCGAGGTCGAGAATTTTATCTGCTGGGCTGCAGGT were used to amplify *sh1*-resistant *MFN2* fragment. In-Fusion cloning (In-Fusion HD Cloning Plus kit, Clontech) was used to fuse the *sh1*-resistant *MFN2* fragment with the linearized backbone. pLKO.1 constructs together with pCMV-dR8.2 dvpr (addgene #8455) and pCMV-VSV-G (addgene #8454) were co-transfected into HEK293T cells with Lipofectamin 3000 (Invitrogen L3000015) to produce lentivirus. Virus supernatant was collected at both 48 hpt and 72 hpt, and further concentrated with Lenti-X concentrator (Clotech 631232). HL-60 cells were infected with concentrated lentivirus in complete medium supplemented with 4 ug/ml polybrene (Sigma TR-1003-G) and then selected with 1 µg/ml puromycin (Gibco A1113803) to generate stable line.

**Microinjection**

Microinjections of fish embryos were performed as described[64]. Briefly, 1 nl of mixture containing 25 ng/µl plasmid and 35 ng/µl Tol2 transposase mRNA was injected into the cytoplasm of embryos at one-cell stage.

**Tailfin wounding and Sudan black staining.** Tailfin wounding and Sudan Black staining were carried out with 3 dpf embryos as described[65]. Briefly, embryos were fixed in 4% paraformaldehyde in phosphate-buffered saline overnight at 4°C and stained with Sudan black.

**Live imaging**

Time-lapse images for zebrafish circulation, $LTB_4$ bath, flow adhesion assay were obtained with AXIO Zoom V16 microscope (Zeiss) at no interval or 30 s interval ($LTB_4$ bath). Time-lapse fluorescence images for zebrafish neutrophil motility were acquired by a laser scanning confocal microscope (LSM 710, Zeiss) with a 1.0/20 x objective lens at 1 min interval of 30 min. Neutrophils were tracked using ImageJ with MTrackJ plugin and the velocity was plotted in Prism 6.0 (GraphPad).

For confocal imaging, images were obtained using a laser-scanning confocal microscope (LSM 800, Zeiss) with a 1.4/63x oil immersion objective lens. Images were analysis with ImageJ.

For fluorescence intensity measurement, images within an experiment were acquired using identical camera settings and background was subtracted by ImageJ with the rolling ball radius as 50. Mean fluorescence intensity of interested areas was measured by Measurement in ImageJ and plotted in Prism (GraphPad) software. For colocalization analysis, background was subtracted in both channels using ImageJ with the rolling ball radius as 50. Images were then

processed by Coloc 2 of ImageJ to calculate the colocalization. Interaction between channels was quantified by Manders' colocalization coefficient as described[30].

**Adhesion assay**

Adhesion assay was performed as described[66]. Differentiated HL-60 cells were resuspended in mHBSS (HBSS with 0.5% FBS and 20 mM HEPES) and plated in 96-well plate (greiner bio-one 655069) coated with 10 µg/ml fibrinogen (sigma F3879) for 1 h with 20,000 cells /well. Cells were incubated at 37$^{o}$C for 15 min. PBS or fMLP (sigma F3506) at a final concentration of 100 nM was added to each well, and cells were incubated for another 15 min. Then cells were gently agitated and wash with mHBSS twice to remove unattached cells, and stained with 0.5% crystal violet with 4% paraformaldehyde for 30 min at room temperature. Adhesion of cells was assessed by measurement of absorbance at 570 nm.

**µ-slide Chemotaxis**

Differentiated HL-60 cells were resuspended in mHBSS at 4x10$^{6}$/ml and loaded into µ-slides (ibidi, 80322) following manufacturer's instructions. fMLP was added to the right reservoir at a concentration of 1 µM. Chemotaxis was recorded every 1 min for 2 h using a laser scanning confocal microscope (LSM 710, Zeiss) with a 1.0/10 x objective. The velocity of neutrophils was measured using ImageJ with MTrackJ plugin and plotted in Prism 6.0 (GraphPad). For inhibitor treatments, dHL-cells were pre-treated with DMSO, NSC23766 (200 µM, Sigma SML0952), AIP (50 µM, R&D SYSTEMS 5959/1) or CAS 1090893 (50 µM, Millipore 553511) for 30 min before loading into µ-slides.

**Flow adhesion**

Neutrophil flow adhesion assay was performed as described[67]. Briefly, $5x10^5$ HUVEC cells in 2 ml were plated onto 10 ug/ml fibrinogen-coated 35 mm plate (Corning 430165), and incubated at 37$^o$C. Then the HUVEC monolayer was primed by 20 ng/ml human TNF-a (Life technologies PHC3015) for 4-6 h. dHL-60 cells were harvested and resuspended at a cell density of $5x10^5$ cells/ml in complete medium. dHL-60 cells were flowed on top of HUVEC monolayer at a speed of 350 µl/min using a syringe pump. Cells adhering to the monolayer were recorded using AXIO Zoom V16 microscope (Zeiss) with camera streaming for 5 min. The total number of adherent neutrophils were quantified at 5 min.

**Rac-GTP pulldown assay**

PAK-GST-coated beads (Cytoskeleton BK035) was used to isolate active Rac from whole-cell lysate as described[68]. Briefly, dHL-60 cells were serum starved with RPMI medium lacking FBS for 1 h in the incubator at a density of $2x10^6$ cells/ml. After starvation, cells were pelleted and suspended in mHBSS, and plated on fibrinogen-coated 100 mm tissue culture dish to attach for 30 min. fMLP was then added to the cells at a final concentration of 100 nM, then cells were lysed with ice-cold lysis buffer at indicated time points and collected by scrapples. 10 µg PAK-GST beads were mixed with each sample and incubated at 4$^o$C for 1h. Protein beads were washed and processed for western blot.

**Western Blot**

Protein samples were separated using SDS-PAGE and transferred onto nitrocellulose membranes (LI-COR NC9680617). Membranes were blocked for ~30 min in PBST (PBS and 0.1% Tween

20) with 5% BSA. After blocking, membranes were incubated with primary antibodies diluted 1:1,000 in PBST at 4$^{o}$C for overnight and secondary antibodies diluted 1:10,000 in PBST at room temperature for 1 h. Odyssey (LI-Cor) was used to image membranes. Primary antibodies anti-Mfn2 (Cell Signaling 9482S), anti-Mfn1 (Cell Signaling 14793S), anti-beta-Tubulin (DSHB, E7), anti-Rac1/2/3 (Cell Signaling 2465S) and secondary antibody anti-rabbit (ThermoFisher SA5-35571), anti-mouse (Invitrogen 35518) were used. For active Rac pull down assays, images were analyzed by ImageJ. The ratio of active Rac to total Rac was calculated and normalized to the value of vector control.

**Bone Marrow Neutrophil isolation and western blot**

Femurs and Tibias from mice 8-12 weeks of age were isolated and whole bone marrow was isolated, and passed through a 70 µm filter followed by RBC lysis (Qiagen 158904). Bone marrow neutrophils were isolated using a negative selection column (MACS 130-097-658). Neutrophils viability was determined by trypan blue staining showing >99% viability. 2x10^6 neutrophils were used for western blot to assess *Mfn2* KO (anti-Mfn2, Invitrogen-PA5-42171) efficiency where Vinculin (anti-Vinculin, Sigma V9131) was used as a loading control.

**Peritonitis model**

1ml of 4% thioglycollate (Sigma B2551) was injected directly into the peritoneal cavity of mice 6-8 weeks of age. After 3 hours of incubation, peritoneal ascites were collected by introducing 8 ml of PBS into the cavity and collecting the ascites immediately afterwards. Cells were subjected to RBC lysis and viability was determined via trypan blue staining. Total cells were stained with CD11b (BD 557686) and Ly6G (BD 566453) on ice for 30 minutes and washed 3 times with

staining buffer. Cells profiles were collected with a BD fortessa analyzer and analyzed with Beckman kaluza software. Neutrophil population was defined as FCS/SSC high and CD11b+Ly6G$^{high}$. Percentage of neutrophils in the lavage relative to total viable cells in each experiment was normalized to the sex-matched littermate control.

**Immunostaining**

dHL-60 cells were resuspended in mHBSS and attached to fibrinogen-coated slides for 30 min. Then cells were stimulated with 100 nM fMLP for 3 min and fixed with 3% paraformaldehyde in PBS for 15 min at 37$^{o}$C. The immunostaining of fixed cells were performed as described[69]. Briefly, after fixation, cells were permeabilized in PBS with 0.1% Triton X-100 and 3% BSA for 1 h at room temperature. dHL-60 cells were incubated with phalloidin -AlexaFluor 488 (Invitrogen A12379) or primary antibodies diluted 1:100 in 3% BSA overnight at 4 $^{o}$C. The cells were then stained with secondary antibodies diluted 1:500 in 3% BSA and DAPI (Invitrogen D3571) for 1 h at room temperature. Images were acquired using LSM 800 (Zeiss) and processed with ImageJ. For MEF staining, cells were plated onto fibrinogen-coated slides and incubated for ~4 h at 37 $^{o}$C, followed with fixation with 3% paraformaldehyde in PBS. Primary antibodies anti-Mfn2 (Cell Signaling 9482S), anti-TOMM20 (Santa Cruz sc-17764), anti-Calnexin (ThermoFisher MA3-027), anti-Tubulin (Sigma T5168), anti-Paxillin (Invitrogen AHO0492), anti-RAC-GTP (NewEast Biosciences 26903), anti-p-CaMKII (Cell Signaling 12716S), anti-Tiam2 (Abcam ab199426), and secondary antibody anti-rabbbit AlexaFluor 568 (Invitrogen A-11011), anti-mouse AlexaFluor 647 (Invitrogen A21236) were used.

**Electron microscopy**

Transmission Electron Microscopy was performed at Purdue Life Science Microscopy Facility. dHL-60 cells were pelleted and fixed in 2.5% glutaraldehyde in 0.1 M sodium cacodylate buffer, post-fixed in buffered 1% osmium tetroxide containing 0.8% potassium ferricyanide, and en bloc stained in 1% aqueous uranyl acetate. They were then dehydrated with a graded series of acetonitrile and embedded in EMbed-812 resin. Thin sections (80nm) were cut on a Leica EM UC6 ultramicrotome and stained with 2% uranyl acetate and lead citrate. Images were acquired using a Gatan US1000 2K CCD camera on a FEI Tecnai G2 20 electron microscope equipped with a LaB6 source and operating at 100 kV or 200kV.

**$Ca^{2+}$ measurement**

Fluo-4 Calcium Imaging Kit (Invitrogen F10489) was used for cytosolic $Ca^{2+}$ measurement. dHL-60 cells were resuspended in mHBSS and incubated with PowerLoad solution and Fluo-4 dye at 37 $^{o}$C for 15 min and then at room temperature for 15 min. After incubation, cells were washed with mHBSS and loaded into fibrinogen-coated 96-well plates (greiner bio-one 655069) with 20,000 cells in 150 ul for each well, followed by incubation at 37 $^{o}$C for 30 min. Green fluorescence images were recorded by BioTek Lionheart FX Automated Microscope with 20x phase lens at 1s interval of 10s. Then 15 ul of 1 uM fMLP was injected into cells using the injector of BioTek Lionheart FX Automated Microscope. Images were recorded for another 2 min with 1s interval. The fluorescence intensity of basal $Ca^{2+}$ level was set to 0.

For mitochondrial $Ca^{2+}$ measurement, Rhod-2 (Invitrogen R1245MP) was used. dHL-60 cells were incubated in mHBSS with Rhod-2 at 37 $^{o}$C for 30 min, and then washed and added into fibrinogen-coated 96-well plates with 150 µl/well. After 30 min incubation, time-lapse red fluorescence images were acquired by BioTek Lionheart FX Automated Microscope with 1s

interval of 10s and followed by fMLP injection and image recording for another 2 min with 1s interval. The fluorescence intensity of basal $Ca^{2+}$ was normalized to 0.

**Cell spreading**

MEF cell spreading assay was performed as described[70]. Briefly, cells were trypsinized and replated onto fibrinogen-coated µ-slide 8 well plates (ibidi 80826) with complete medium. Time-lapse images were acquired using BioTek Lionheart FX Automated Microscope with 20x phase lens at 2 min interval of ~3 h at 37°C with 5% $CO_2$.

**Wound closure**

MEF cells in complete medium were seeded onto 96-well plates (FALCON 353075) and incubated at 37 $^{o}$C overnight. A wound was induced by automated 96-well WoundScratcher (BioTek) for each well. Cells were washed twice with mHBSS and time-lapse images were acquired using BioTek Lionheart FX Automated Microscope with 4x phase lens at 20 min interval of ~12 h at 37°C with 5% $CO_2$.

**Flow cytometry analysis**

dHL-60 cells were harvested and resuspended into ice-cold FACS buffer (PBS with 1% BSA) at a concentration of $1x10^6$ cells/ml. 5 ul of Annexin V (BD 563973) solution were added into 100 ul cell suspension and incubated at room temperature for 30 min. Cells were washed for three times with ice-cold FACS buffer, and followed by flow cytometry analysis.

**Mitochondrial membrane potential, ROS, and ATP measurement**

Mitochondrial membrane potential was measured using TMRM. dHL-60 cells were resuspended in mHBSS and incubated with 150 nM MitoTracker (Invitrogen M22426), 20 nM TMRM (Invitrogen T668), and 0.2 µg/ml Hoechst (Invitrogen H3570) for 30 min at 37 $^{o}$C. Then cells were washed and plated onto fibrinogen-coated µ-slide 8 well plates. After 30 min incubation, cells were stimulated with or without fMLP at a concentration of 100 nM. The fluorescent images were acquired using BioTek Lionheart FX Automated Microscope with 20x phase lens, and processed using ImageJ. Mitochondrial membrane potential was measured using the fluorescence intensity of TMRM normalized to the intensity of MitoTracker of each cell. For mitochondrial ROS measurement, MitoSOX (M36008) was used. 5 µM of mitoROX was added to the cell suspension and incubated for 30 min at 37 $^{o}$C. Cellular ATP level was measured using ATP Assay Kit (abcam #ab83355) according to the assay procedure. Briefly, dHL-60 cells treated with or without fMLP were harvested, washed with PBS, and resuspended in ATP Assay Buffer. Samples with ATP reaction mix were loaded into 96-well plate (greiner bio-one 655069) and incubated at room temperature for 30 min protected from light. Results were measured using a microplate reader (BioTek) at Ex/Em = 535/587. All results were normalized to control cell lines without fMLP treatment.

**Mutational Efficiency Quantification**

The mutation efficiency of neutrophil-specific knockout in zebrafish was quantified as described[63]. To determine the mutation efficiency in *Tg(lyzC:Cas9-mfn2 sgRNAs)*, *Tg(lyzC:Cas9-mfn2 sgRNAs#2)*, and *Tg(lyzC:Cas9-opa1 sgRNAs)*, 3 dpf embryos of each line were digested with trypsin to prepare single cell suspensions. mCherry positive cells were sorted by FACS. Genomic DNA was purified using QIAamp DNA Mini Kit (Qiagen) from sorted cells.

5 µg of poly(dA:dT) (Invivogen) were used as the carrier DNA. The *mfn2 and opa1* loci around the sgRNA binding sites were amplified using PCR with the following primers: mfn2-F1: GGCGATGATAAACATGGCAGTTTG, mfn2-R1: GTACCACAGGTGCACAGTGTC, mfn2-F2: CTGGGACGCATCGGCCAATG, mfn2-R2: CTACCTGCTTCAGGCATTCCCTG, mfn2#2-F1: GTCGGGCTTCTCCTAAGTTATTC, mfn2#2-R1: CAGTGTCCATAGCCTAGAGTCTGC, mfn2#2-F2: GTGGTCTCATATAATTTTGCTTGCTG, mfn2#2-R2: CACACGCGAATCGATAAGAGGAAT, opa1-F1: CAAGCTCATTAAAGGTTTGAAACCACTTG, opa1-R1: CTCCACAAATCACATAGGTGAC, opa1-F2: GTGCCTGAATGCTCTACACTTTC, opa1-R: CATGATAACAATACCATGCACATGC, Purified PCR products were used for library construction with Nextera library prep kit and sequenced using an Illumina MiSeq 300 at the sequencing center of Purdue University. Raw reads have been deposited to the Sequence Read Archive (Accession number PRJNA510381, https://www.ncbi.nlm.nih.gov/Traces/study/?acc=SRP132222). Mutational efficiency was calculated using the CrispRVariants R package (Lindsay et al., 2016).

**Statistical analysis**

Statistical analysis was performed with Prism 6 (GraphPad). Two-tailed student's *t* test, or ANOVA was used to determine the statistical significance of differences between groups. A *P* value of less than 0.05 indicated in the figures by asterisks was considered as statistically significant.

## References

1. Gambardella, L. & Vermeren, S. Molecular players in neutrophil chemotaxis--focus on PI3K and small GTPases. *J Leukoc Biol* **94**, 603-612 (2013).
2. Mocsai, A., Walzog, B. & Lowell, C.A. Intracellular signalling during neutrophil recruitment. *Cardiovasc Res* **107**, 373-385 (2015).
3. de Oliveira, S., Rosowski, E.E. & Huttenlocher, A. Neutrophil migration in infection and wound repair: going forward in reverse. *Nature reviews. Immunology* **16**, 378-391 (2016).
4. Pantarelli, C. & Welch, H.C.E. Rac-GTPases and Rac-GEFs in neutrophil adhesion, migration and recruitment. *Eur J Clin Invest* **48 Suppl 2**, e12939 (2018).
5. Futosi, K., Fodor, S. & Mocsai, A. Neutrophil cell surface receptors and their intracellular signal transduction pathways. *International immunopharmacology* **17**, 638-650 (2013).
6. Tsai, F.C., Kuo, G.H., Chang, S.W. & Tsai, P.J. Ca2+ signaling in cytoskeletal reorganization, cell migration, and cancer metastasis. *Biomed Res Int* **2015**, 409245 (2015).
7. Price, L.S. *et al.* Calcium signaling regulates translocation and activation of Rac. *The Journal of biological chemistry* **278**, 39413-39421 (2003).
8. Campello, S. & Scorrano, L. Mitochondrial shape changes: orchestrating cell pathophysiology. *EMBO Rep* **11**, 678-684 (2010).
9. Campello, S. *et al*. Orchestration of lymphocyte chemotaxis by mitochondrial dynamics. *Journal of Experimental Medicine* **203**, 2879-2886 (2006).

10. Zhao, J. *et al.* Mitochondrial dynamics regulates migration and invasion of breast cancer cells. *Oncogene* **32**, 4814-4824 (2013).

11. Borregaard, N. & Herlin, T. Energy metabolism of human neutrophils during phagocytosis. *The Journal of clinical investigation* **70**, 550-557 (1982).

12. Peachman, K.K., Lyles, D.S. & Bass, D.A. Mitochondria in eosinophils: functional role in apoptosis but not respiration. *Proc Natl Acad Sci U S A* **98**, 1717-1722 (2001).

13. Fossati, G. *et al.* The mitochondrial network of human neutrophils: role in chemotaxis, phagocytosis, respiratory burst activation, and commitment to apoptosis. *Journal of immunology* **170**, 1964-1972 (2003).

14. Bao, Y. *et al.* Mitochondria regulate neutrophil activation by generating ATP for autocrine purinergic signaling. *The Journal of biological chemistry* **289**, 26794-26803 (2014).

15. Bao, Y. *et al.* mTOR and differential activation of mitochondria orchestrate neutrophil chemotaxis. *The Journal of cell biology* **210**, 1153-1164 (2015).

16. Li, X.O. *et al.* Removal of extracellular ATP improves fMLP-induced neutrophil chemotaxis. *Eur Respir J* **48** (2016).

17. Schuler, M.H. *et al.* Miro1-mediated mitochondrial positioning shapes intracellular energy gradients required for cell migration. *Molecular biology of the cell* **28**, 2159-2169 (2017).

18. Zanotelli, M.R. *et al.* Regulation of ATP utilization during metastatic cell migration by collagen architecture. *Molecular biology of the cell* **29**, 1-9 (2018).

19. Bi, D., Lopez, J.H., Schwarz, J.M. & Manning, M.L. Energy barriers and cell migration in densely packed tissues. *Soft matter* **10**, 1885-1890 (2014).

20. Zhou, W. *et al.* Neutrophil-specific knockout demonstrates a role for mitochondria in regulating neutrophil motility in zebrafish. *Disease models & mechanisms* **11** (2018).

21. Maianski, N.A., Mul, F.P., van Buul, J.D., Roos, D. & Kuijpers, T.W. Granulocyte colony-stimulating factor inhibits the mitochondria-dependent activation of caspase-3 in neutrophils. *Blood* **99**, 672-679 (2002).

22. Chen, H. *et al.* Mitofusins Mfn1 and Mfn2 coordinately regulate mitochondrial fusion and are essential for embryonic development. *The Journal of cell biology* **160**, 189-200 (2003).

23. Song, Z., Chen, H., Fiket, M., Alexander, C. & Chan, D.C. OPA1 processing controls mitochondrial fusion and is regulated by mRNA splicing, membrane potential, and Yme1L. *The Journal of cell biology* **178**, 749-755 (2007).

24. Harvie, E.A. & Huttenlocher, A. Neutrophils in host defense: new insights from zebrafish. *Journal of leukocyte biology* **98**, 523-537 (2015).

25. Chen, H., McCaffery, J.M. & Chan, D.C. Mitochondrial fusion protects against neurodegeneration in the cerebellum. *Cell* **130**, 548-562 (2007).

26. Abram, C.L., Roberge, G.L., Pao, L.I., Neel, B.G. & Lowell, C.A. Distinct roles for neutrophils and dendritic cells in inflammation and autoimmunity in motheaten mice. *Immunity* **38**, 489-501 (2013).

27. Luchsinger, L.L., de Almeida, M.J., Corrigan, D.J., Mumau, M. & Snoeck, H.W. Mitofusin 2 maintains haematopoietic stem cells with extensive lymphoid potential. *Nature* **529**, 528-531 (2016).

28. Hall, A. Rho GTPases and the actin cytoskeleton. *Science* **279**, 509-514 (1998).

29. Naon, D. *et al.* Critical reappraisal confirms that Mitofusin 2 is an endoplasmic reticulum-mitochondria tether. *Proceedings of the National Academy of Sciences of the United States of America* **113**, 11249-11254 (2016).

30. de Brito, O.M. & Scorrano, L. Mitofusin 2 tethers endoplasmic reticulum to mitochondria. *Nature* **456**, 605-610 (2008).

31. Glancy, B., Willis, W.T., Chess, D.J. & Balaban, R.S. Effect of calcium on the oxidative phosphorylation cascade in skeletal muscle mitochondria. *Biochemistry-Us* **52**, 2793-2809 (2013).

32. Amini, P. *et al.* Neutrophil extracellular trap formation requires OPA1-dependent glycolytic ATP production. *Nature communications* **9**, 2958 (2018).

33. Marks, P.W. & Maxfield, F.R. Transient Increases in Cytosolic Free Calcium Appear to Be Required for the Migration of Adherent Human-Neutrophils. *Journal of Cell Biology* **110**, 43-52 (1990).

34. Mandeville, J.T.H. & Maxfield, F.R. Effects of buffering intracellular free calcium on neutrophil migration through three-dimensional matrices. *Journal of cellular physiology* **171**, 168-178 (1997).

35. Easley, C.A.t., Brown, C.M., Horwitz, A.F. & Tombes, R.M. CaMK-II promotes focal adhesion turnover and cell motility by inducing tyrosine dephosphorylation of FAK and paxillin. *Cell Motil Cytoskeleton* **65**, 662-674 (2008).

36. Si, J., Mueller, L. & Collins, S.J. CaMKII regulates retinoic acid receptor transcriptional activity and the differentiation of myeloid leukemia cells. *The Journal of clinical investigation* **117**, 1412-1421 (2007).

37. Fleming, I.N., Elliott, C.M., Buchanan, F.G., Downes, C.P. & Exton, J.H. Ca2+/calmodulin-dependent protein kinase II regulates Tiam1 by reversible protein phosphorylation. *J Biol Chem* **274**, 12753-12758 (1999).

38. Rooney, C. *et al.* The Rac activator STEF (Tiam2) regulates cell migration by microtubule-mediated focal adhesion disassembly. *EMBO reports* **11**, 292-298 (2010).

39. Boespflug, N.D. *et al.* ATF3 is a novel regulator of mouse neutrophil migration. *Blood* **123**, 2084-2093 (2014).

40. Eisenberg-Bord, M., Shai, N., Schuldiner, M. & Bohnert, M. A Tether Is a Tether Is a Tether: Tethering at Membrane Contact Sites. *Developmental cell* **39**, 395-409 (2016).

41. Zuchner, S. *et al.* Mutations in the mitochondrial GTPase mitofusin 2 cause Charcot-Marie-Tooth neuropathy type 2A. *Nature genetics* **36**, 449-451 (2004).

42. Filadi, R., Pendin, D. & Pizzo, P. Mitofusin 2: from functions to disease. *Cell death & disease* **9**, 330 (2018).

43. Chandhok, G., Lazarou, M. & Neumann, B. Structure, function, and regulation of mitofusin-2 in health and disease. *Biological reviews of the Cambridge Philosophical Society* **93**, 933-949 (2018).

44. Lugus, J.J., Ngoh, G.A., Bachschmid, M.M. & Walsh, K. Mitofusins are required for angiogenic function and modulate different signaling pathways in cultured endothelial cells. *J Mol Cell Cardiol* **51**, 885-893 (2011).

45. Hind, L.E., Vincent, W.J. & Huttenlocher, A. Leading from the Back: The Role of the Uropod in Neutrophil Polarization and Migration. *Dev Cell* **38**, 161-169 (2016).

46. Houk, A.R. *et al.* Membrane tension maintains cell polarity by confining signals to the leading edge during neutrophil migration. *Cell* **148**, 175-188 (2012).

47. Ridley, A.J. Rho GTPases and cell migration. *J Cell Sci* **114**, 2713-2722 (2001).

48. Fayngerts, S.A. *et al.* Direction of leukocyte polarization and migration by the phosphoinositide-transfer protein TIPE2. *Nat Immunol* **18**, 1353-1360 (2017).

49. Johnsson, A.E. *et al.* The Rac-FRET mouse reveals tight spatiotemporal control of Rac activity in primary cells and tissues. *Cell reports* **6**, 1153-1164 (2014).

50. Sander, E.E., ten Klooster, J.P., van Delft, S., van der Kammen, R.A. & Collard, J.G. Rac downregulates Rho activity: reciprocal balance between both GTPases determines cellular morphology and migratory behavior. *J Cell Biol* **147**, 1009-1022 (1999).

51. Zhao, Z.S., Manser, E., Loo, T.H. & Lim, L. Coupling of PAK-interacting exchange factor PIX to GIT1 promotes focal complex disassembly. *Mol Cell Biol* **20**, 6354-6363 (2000).

52. Huttenlocher, A. & Horwitz, A.R. Integrins in cell migration. *Cold Spring Harbor perspectives in biology* **3**, a005074 (2011).

53. Wang, S. *et al.* Tiam1 interaction with the PAR complex promotes talin-mediated Rac1 activation during polarized cell migration. *J Cell Biol* **199**, 331-345 (2012).

54. Prudent, J. *et al.* Mitochondrial Ca(2+) uptake controls actin cytoskeleton dynamics during cell migration. *Scientific reports* **6**, 36570 (2016).

55. Giannone, G., Ronde, P., Gaire, M., Haiech, J. & Takeda, K. Calcium oscillations trigger focal adhesion disassembly in human U87 astrocytoma cells. *Journal of Biological Chemistry* **277**, 26364-26371 (2002).

56. Conklin, M.W., Lin, M.S. & Spitzer, N.C. Local calcium transients contribute to disappearance of pFAK, focal complex removal and deadhesion of neuronal growth cones and fibroblasts. *Developmental biology* **287**, 201-212 (2005).

57. Price, L.S. *et al.* Calcium signaling regulates translocation and activation of Rac. *Journal of Biological Chemistry* **278**, 39413-39421 (2003).

58. Geijsen, N. *et al.* Regulation of p21rac activation in human neutrophils. *Blood* **94**, 1121-1130 (1999).

59. Fleming, I.N., Elliott, C.M., Buchanan, F.G., Downes, C.P. & Exton, J.H. Ca2+/calmodulin-dependent protein kinase II regulates Tiam1 by reversible protein phosphorylation. *Journal of Biological Chemistry* **274**, 12753-12758 (1999).

60. Franco, S.J. *et al.* Calpain-mediated proteolysis of talin regulates adhesion dynamics. *Nat Cell Biol* **6**, 977-983 (2004).

61. Lee, S.Y. *et al.* Regulation of the interaction between PIPKI gamma and talin by proline-directed protein kinases. *J Cell Biol* **168**, 789-799 (2005).

62. Hendey, B., Lawson, M., Marcantonio, E.E. & Maxfield, F.R. Intracellular calcium and calcineurin regulate neutrophil motility on vitronectin through a receptor identified by antibodies to integrins alpha v and beta 3. *Blood* **87**, 2038-2048 (1996).

63. Zhou, W.Q. *et al.* Neutrophil-specific knockout demonstrates a role for mitochondria in regulating neutrophil motility in zebrafish. *Disease models & mechanisms* **11** (2018).

64. Deng, Q., Yoo, S.K., Cavnar, P.J., Green, J.M. & Huttenlocher, A. Dual roles for Rac2 in neutrophil motility and active retention in zebrafish hematopoietic tissue. *Developmental cell* **21**, 735-745 (2011).

65. Zhou, W.Q. *et al.* MicroRNA-223 Suppresses the Canonical NF-kappa B Pathway in Basal Keratinocytes to Dampen Neutrophilic Inflammation. *Cell Rep* **22**, 1810-1823 (2018).

66. Liu, L.H. *et al*. Radil controls neutrophil adhesion and motility through beta 2-integrin activation. *Mol Biol Cell* **23**, 4751-4765 (2012).

67. Zhou, Y.B., Kucik, D.F., Szalais, A.J. & Edberg, J.C. Human Neutrophil Flow Chamber Adhesion Assay. *Jove-J Vis Exp* (2014).

68. Graziano, B.R. *et al.* A module for Rac temporal signal integration revealed with optogenetics. *Journal of Cell Biology* **216**, 2515-2531 (2017).

69. Fayngerts, S.A. *et al.* Direction of leukocyte polarization and migration by the phosphoinositide-transfer protein TIPE2. *Nature immunology* **18**, 1353-+ (2017).

70. Jovic, M., Naslavsky, N., Rapaport, D., Horowitz, M. & Caplan, S. EHD1 regulates beta 1 integrin endosomal transport: effects on focal adhesions, cell spreading and migration. *J Cell Sci* **120**, 802-814 (2007).

**Acknowledgements:** The clonal HL-60 cell line was generated by Alba Diz-Munoz (EMBL Heidelberg) and a generous gift from the laboratory of Orion Weiner (UCSF). Mice work was initiated with the generous help from Dr. Yao Liu in the laboratory of Zhao-Qing Luo (Purdue). The work was supported by National Institutes of Health [R35GM119787 to DQ], [R01HD073156 to DM] and [P30CA023168 to Purdue Center for Cancer Research] for shared resources. WZ is supported by Cagiantas Fellowship, Purdue University. AH is supported by Purdue Research Foundation Grant.

**Author contributions**: WZ, MNS, DU and DQ designed research and wrote the manuscript. WZ, AH, TW, HM, XW performed experiments. WZ, AH, TW, JJ, HM analyzed data. All authors read and approved the manuscript.

**Competing interests:**

The authors declare no competing interests.

**Data availability statement:**

Plasmids are available on Addgene: p3E-U6a-U6c-mfn2 guide (Plasmid #121993); p3E-U6a-U6c-mfn2 guide#2 (Plasmid #121994); p3E-U6a-U6c-opa1 guide (Plasmid #121995); MYs-IRES-mitoRFP (Plasmid #121996); pMYs-MFN2-IRES-mitoRFP (Plasmid #121997).

## Figures

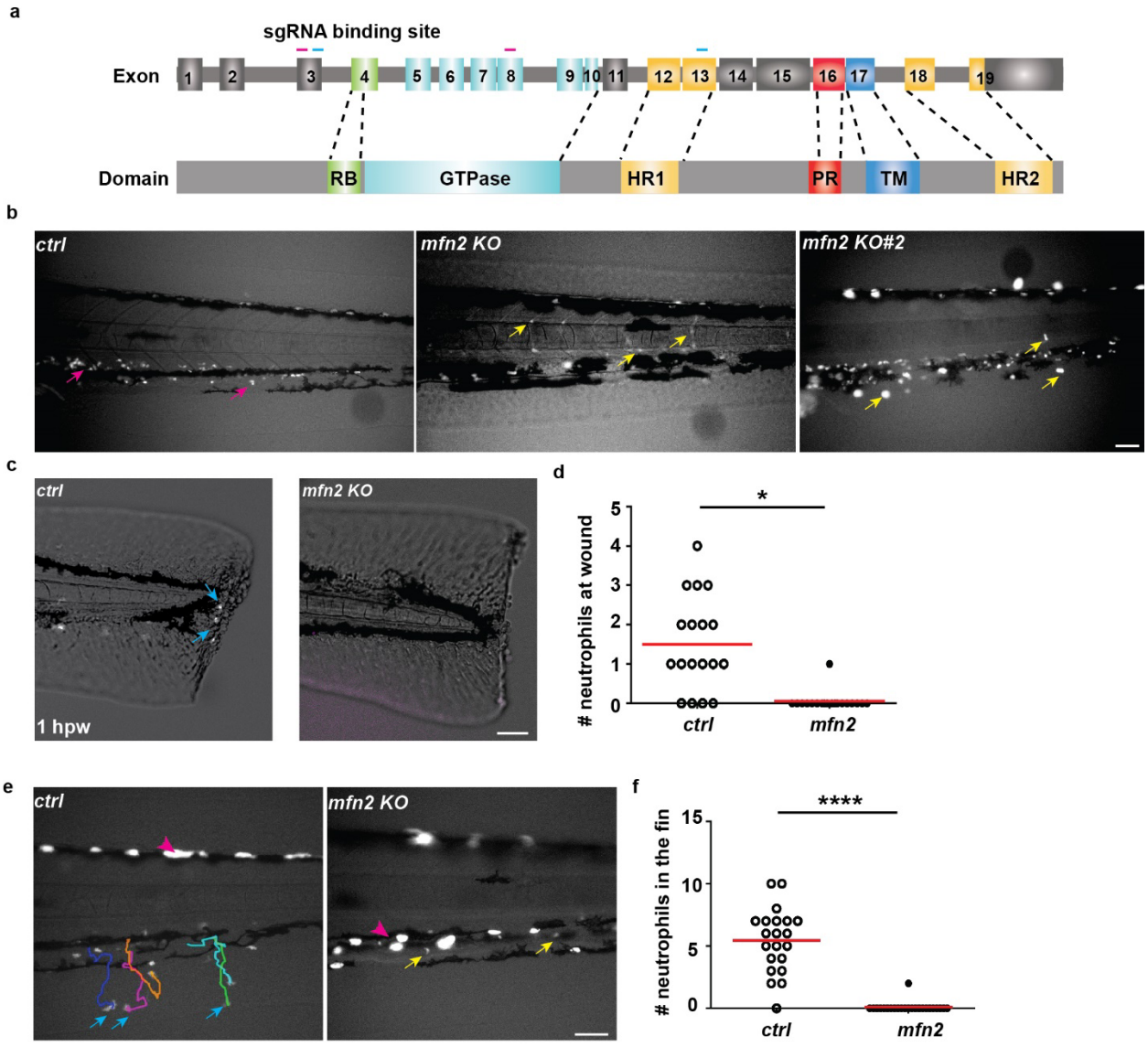


**Figure 1. Mfn2 regulates neutrophil homeostasis in zebrafish.** a) Schematics of the gene structure and protein domains of the zebrafish *mfn2* gene. The first set of sgRNAs (purple lines) targets exon 3 and exon 8 in the forward strand, and the second set (blue lines) targets exon 3 and exon 13 in the forward strand. b) Representative images of neutrophils in the zebrafish trunk of the transgenic lines with neutrophil specific *mfn*2 disruption at 3 dpf. Magenta arrows: neutrophils in the caudal hematopoietic tissue; yellow arrows: neutrophils in the vasculature. c)

Representative images and d) quantification of neutrophil recruitment to the wound edge at 1 hpw. Blue arrows: neutrophils migrated to the wound. e) Representative tracks and f) quantification of neutrophil recruitment to the fin at 30 min post $LTB_4$ treatment. Blue arrows: neutrophils in the fin. One representative result of three biological repeats is shown in d and f. *, $p<0.05$, ****, $p<0.0001$, unpaired *t*-test. Scale bar: 50 μm.

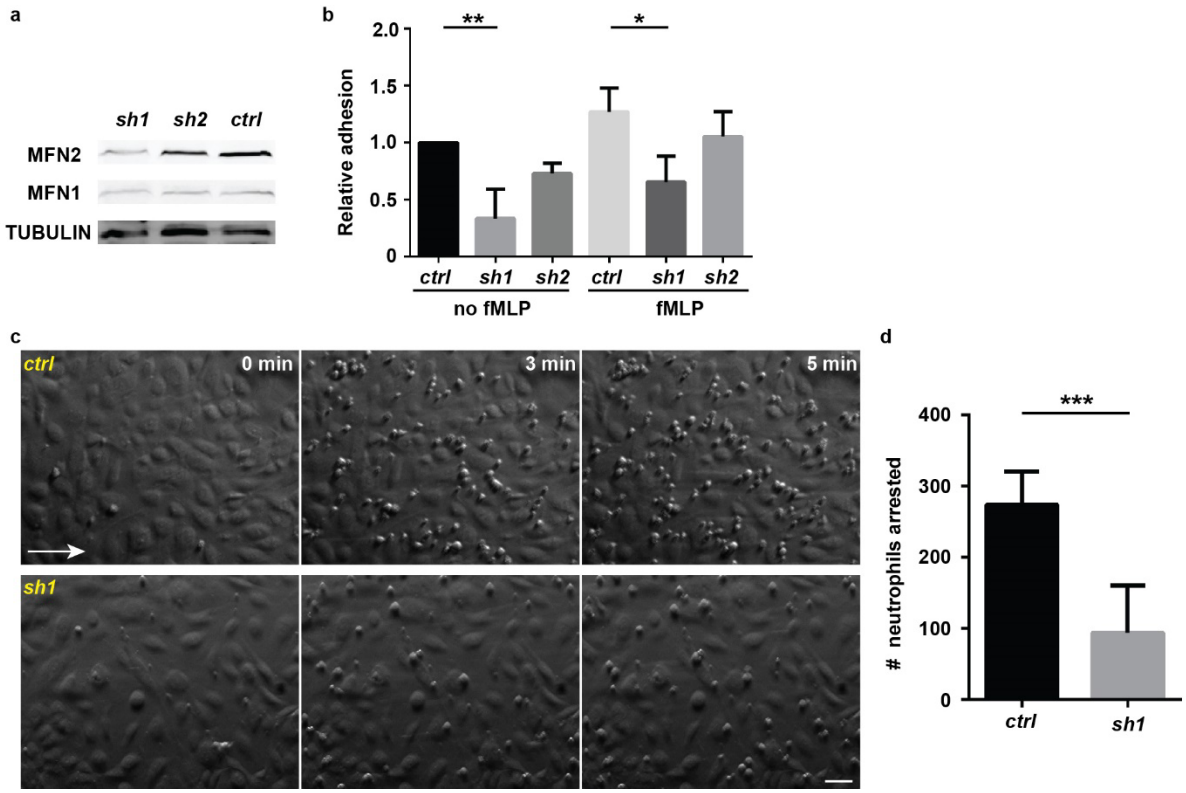


**Figure 2. MFN2 regulates adhesion of dHL-60 cells.** a) Western blot determining the expression level of MFN2 in indicated cell lines. *ctrl*: standard control shRNA; *sh1*: shRNA targeting MFN2; *sh2*, another shRNA targeting MFN2. b) Relative adhesion of neutrophils to fibrinogen coated substrate in the absence and presence of fMLP. c) and d) Adhesion of neutrophils under sheer stress. HUVEC monolayer was activated with TNFα and neutrophils were flowed on top of the monolayer for 5 min. c) Representative images showing neutrophils arrested by HUVEC at different time points. White arrow: flow direction. d) Quantitation of numbers of neutrophils arrested at 5 min. Data were pooled from three independent experiments. *, $p<0.05$; **, $p<0.01$, one-way ANOVA (b). ***, $p<0.001$, unpaired *t*-test (d). Scale bar: 50 µm.

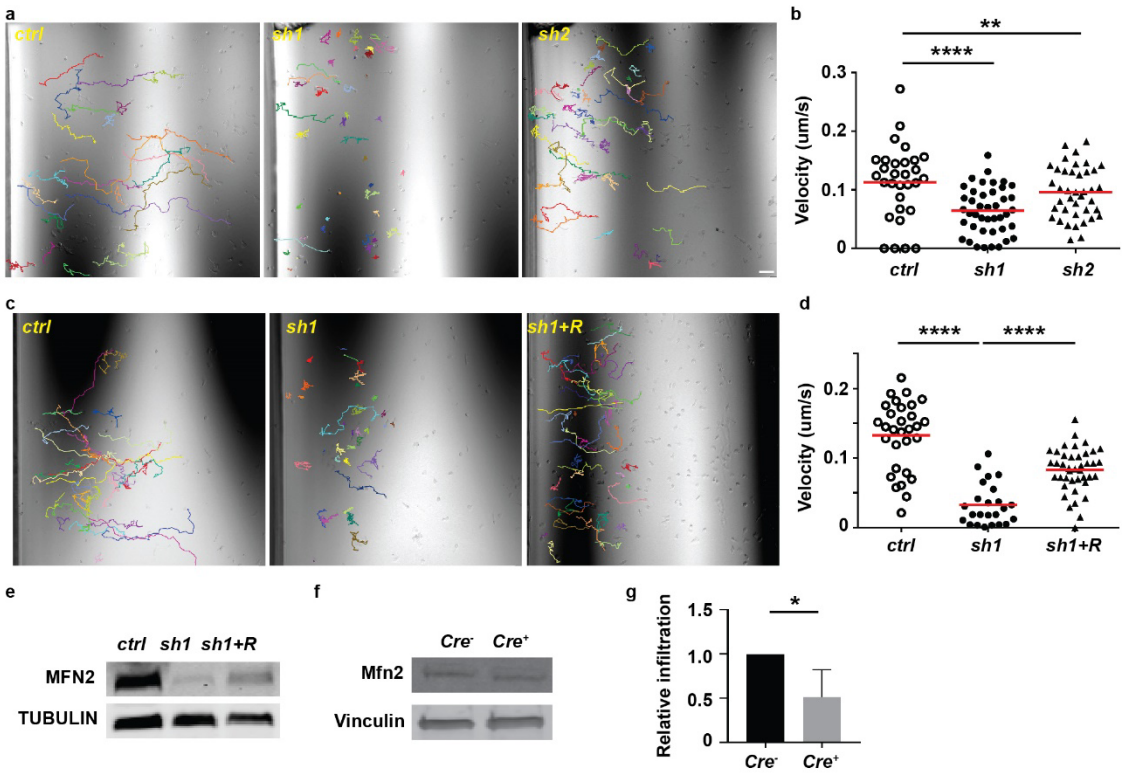


**Figure 3. MFN2 regulates neutrophil migration in vitro and in vivo.** a) Representative images with individual tracks of neutrophil chemotaxis to fMLP. b) Quantification of velocity of neutrophil chemotaxis to fMLP. c) and d) A *sh1* resistant *MFN2* gene was reintroduced to the MFN2 knock down cells expressing *sh1*. c) Quantification and d) Representative images with individual tracks of neutrophils migrating toward fMLP. One representative result of three biological repeats is shown in b and d. **, $p<0.01$, ****, $p<0.0001$, one-way ANOVA. Scale bar: 50 µm. e) Western blot showing the expression level of MFN2 in indicated cell lines. f) Western blot showing the expression level of Mfn2 in mice neutrophils isolated from $Mfn2^{flox/flox}$; *S100A8:Cre+* or the control $Mfn2^{flox/flox}$; *S100A8:Cre-* littermates. g) Neutrophil infiltration to peritoneal cavity in indicated mice. Percentage of neutrophils in the lavage was normalized to that in sex-matched littermates in each experiment. *, $p<0.05$, paired *t*-test.

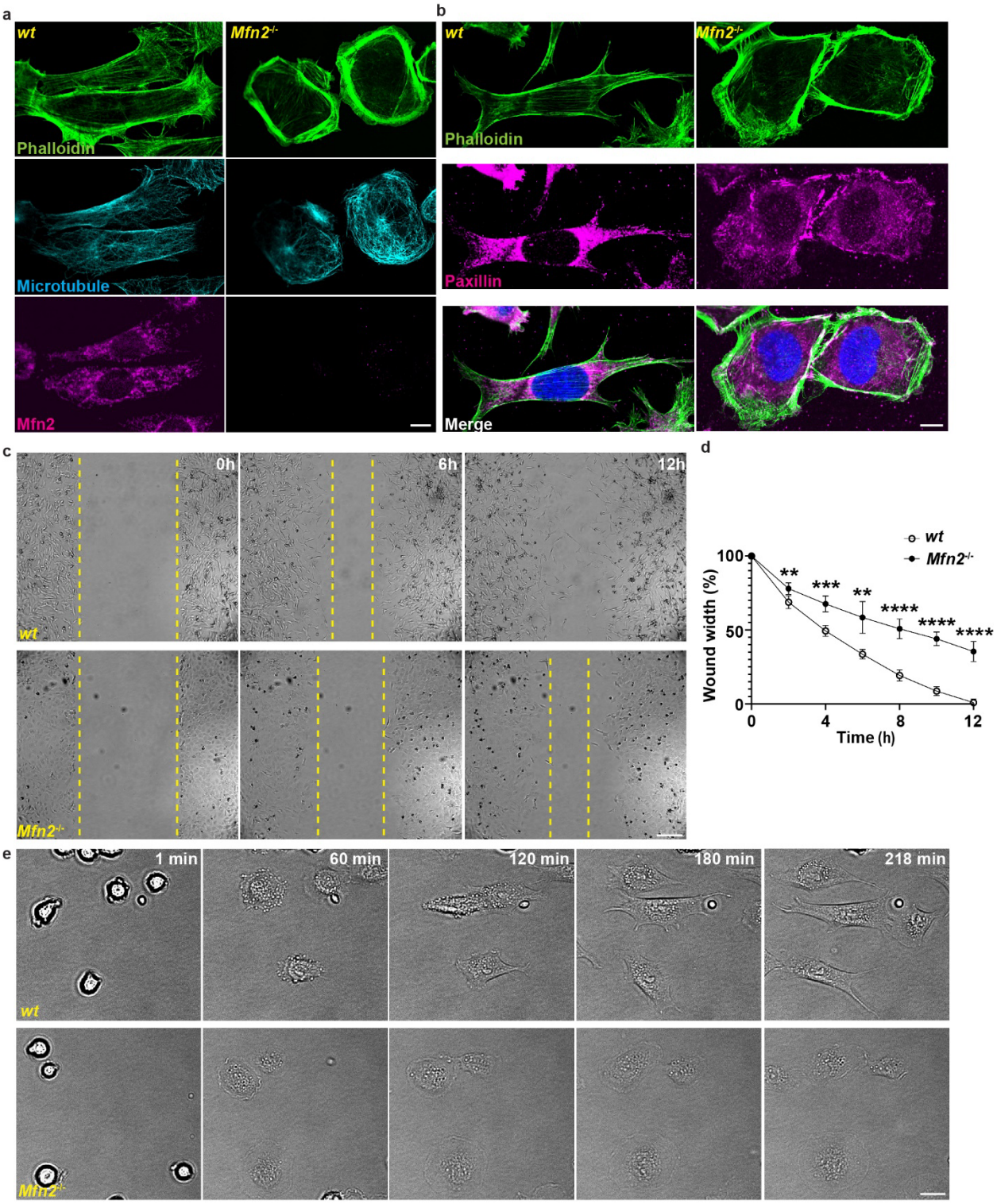


**Figure 4. Mfn2 regulates cytoskeleton organization and cell migration in MEFs.** a) Immunofluorescence of F-actin (phalloidin), microtubule and Mfn2 in *wt* and *Mfn2-null* MEFs. b) Immunofluorescence of F-actin and Paxillin in wt and *Mfn2-null* MEFs. c) Representative

images of wt and *Mfn2-null* MEFs during wound closure at indicated time points. Yellow dash lines: wound edge. d) Quantification of the wound area in wt and *Mfn2-null* MEFs during wound closure. **, p<0.01, ***, p<0.001, ****, p<0.0001unpaired *t*-test. e) Representative images of wt and *Mfn2-null* MEFs during cell spreading at indicated time points. Scale bar: 10 µm (a and b), 20 µm in e and 200 µm in c.

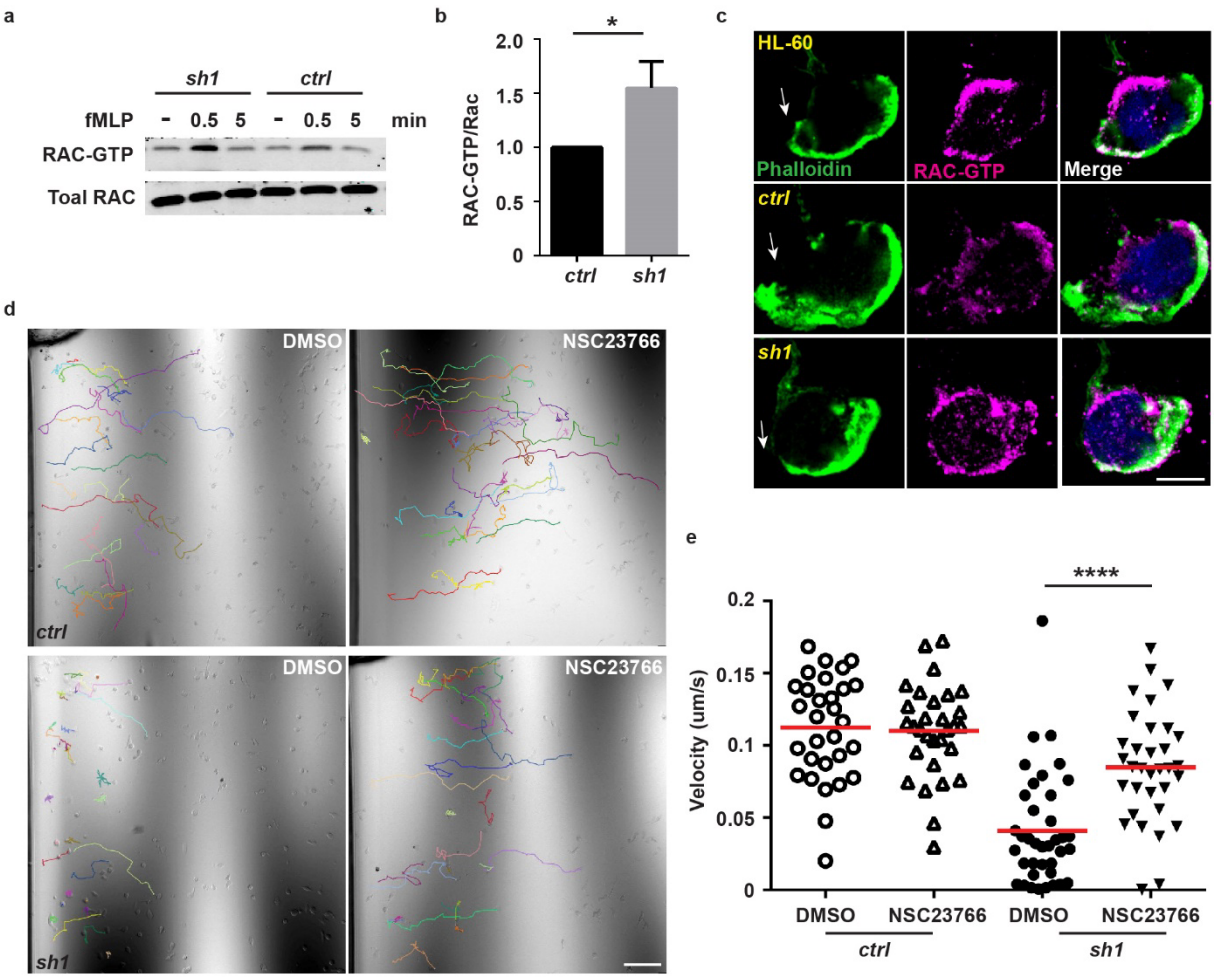


**Figure 5. MFN2 suppresses RAC overactivation in dHL-60 cells.** a) Western blot determining the amount of RAC-GTP and total RAC protein in dHL-60 treated with fMLP at indicated time points. b) Quantification of RAC activation 5 min after stimulation with fMLP. c) Immunofluorescence of F-actin and GTP-RAC in indicated cell lines 3 min after stimulation with fMLP. Arrows: direction of cell polarization. d) Representative images with individual tracks. e) Quantification of velocity of neutrophil chemotaxis to fMLP in the presence of vehicle or the Rac inhibitor NSC23766. Data were pooled from three independent experiments in b. One representative result of three biological repeats was shown in e. *, $p<0.05$; ****, $p<0.0001$, unpaired *t*-test. Scale bar: 10 µm in c; 100 µm in d.

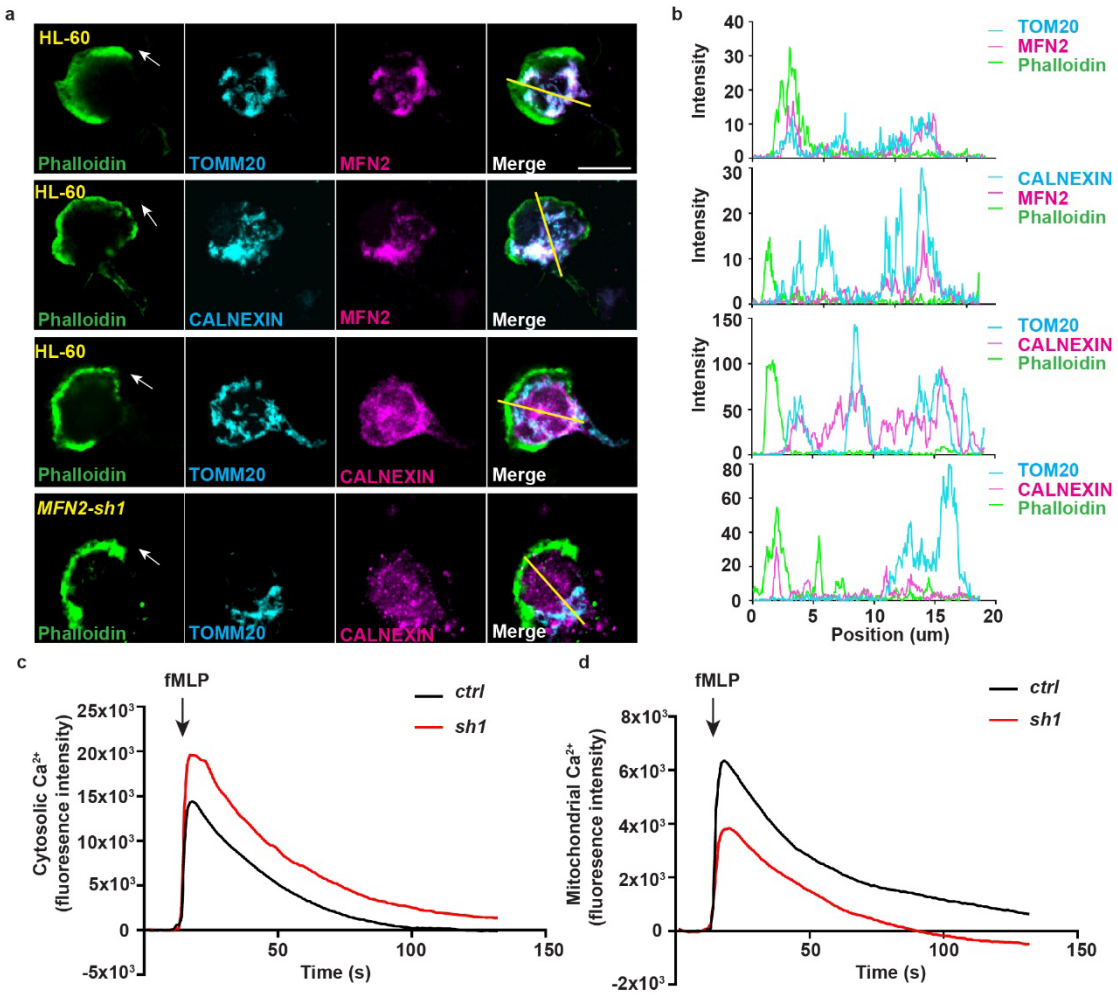


**Figure 6. MFN2 regulates ER-mitochondria interaction and intracellular $Ca^{2+}$.** a) Immunofluorescence of F-actin (phalloidin), mitochondria (TOMM20), MFN2 and ER membrane (CALNEXIN) in indicated cells 3 min post fMLP stimulation. Arrows: direction of cell polarization. b) Plot profiles of the fluorescence intensity (MFI) along the corresponding yellow lines in a. c) Cytosolic $Ca^{2+}$ in the control or MFN2 knockdown cell lines after fMLP stimulation. d) Mitochondrial $Ca^{2+}$ in the control or MFN2 knockdown cell lines after fMLP stimulation. One representative result of three biological repeats is shown in c and d.

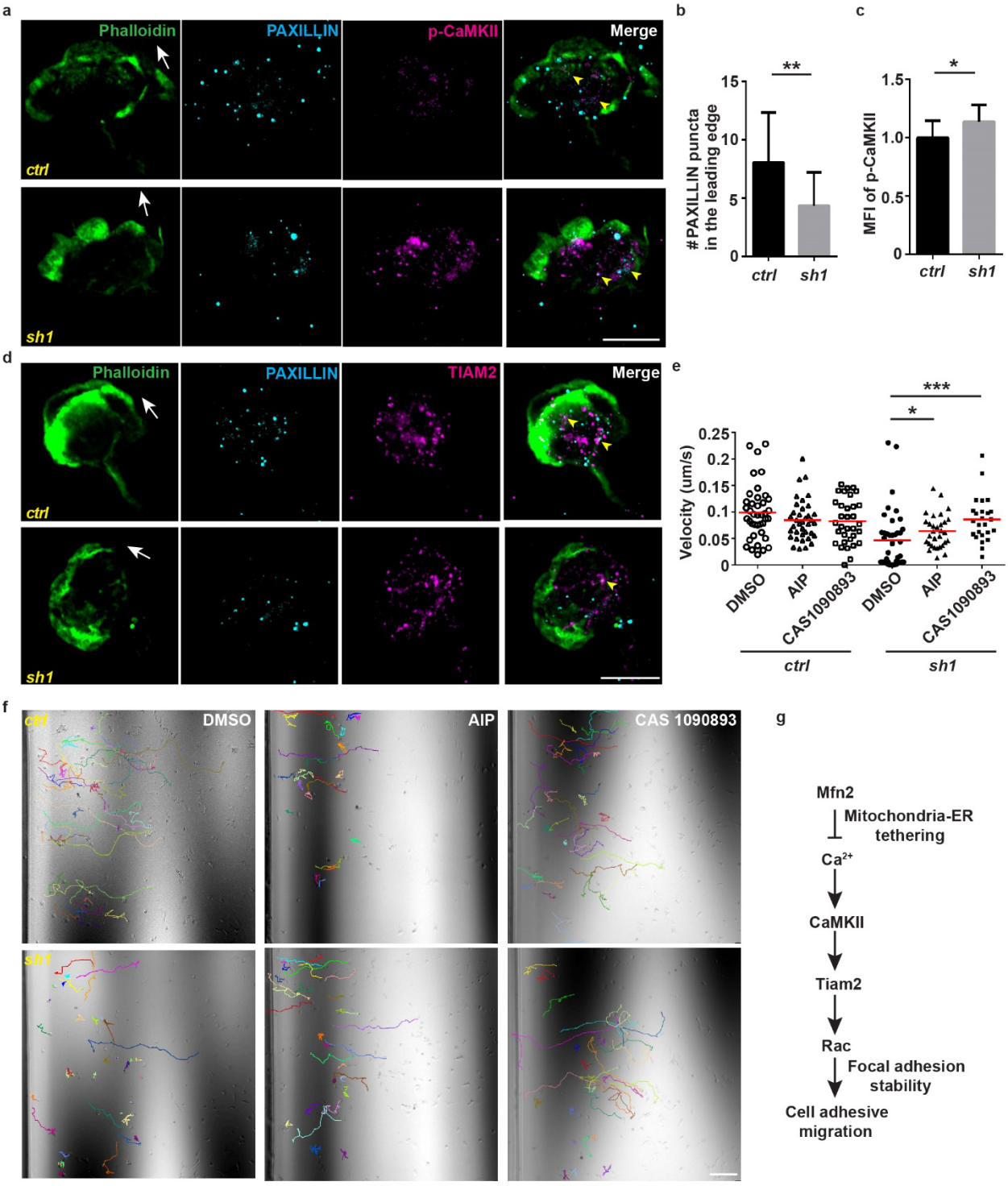


**Figure 7. MFN2 regulates adhesions through CaMKII and TIAM2 in dHL-60 cells.** a) Immunofluorescence of F-actin (phalloidin), PAXILLIN, p-CaMKII in indicated cell lines 3 min post fMLP stimulation. b) Quantification of PAXILLIN puncta at the leading edge of cells. c) Quantification of mean fluorescence intensity of p-CaMKII in the cell body. d)

Immunofluorescence of F-actin (phalloidin) and TIAM2 in indicated dHL-60 cells treated with fMLP. Arrows: the direction of cell polarization; Arrow heads: the close proximity of PAXILLIN and pCAMKII or TIAM. e) Quantification of the velocity and f) representative tracks of dHL-60 cells migrating to fMLP in the presence of vehicle, the CaMK inhibitor AIP or the TIAM inhibitor CAS 1090893. Data were pooled from a total of 17 cells (in b) and 10 cells (in c) in three independent experiments in b and c. One representative result of three biological repeats is shown in e. *, $p<0.05$; **, $p<0.01$, unpaired *t*-test in b and c. *, $p<0.05$; ***, $p<0.001$, one-way ANOVA in e. Scale bar: 10 µm in a and d; 100 µm in f.